# Quantification of hydraulic trait control on plant hydrodynamics and risk of hydraulic failure within a demographic structured vegetation model in a tropical forest (FATES-HYDRO V1.0)

Chonggang Xu[1], Bradley Christoffersen[2], Zachary Robbins[1], Ryan Knox[3], Rosie A. Fisher[4], Rutuja Chitra-Tarak[1], Martijn Slot[5], Kurt Solander[1], Lara Kueppers[3,6], Charles Koven[3], Nate McDowell[7,8]

1: Earth and Environmental Sciences Division, Los Alamos National Laboratory, Los Alamos NM, USA

2: School of Integrative Biological and Chemical Sciences, University of Texas Rio Grande Valley, TX, USA

3: Lawrence Berkeley National Laboratory, Berkeley, CA USA

4. CICERO Centre for International Climate Research, Oslo, Norway

5: Smithsonian Tropical Research Institute, Apartado 0843-03092, Balboa, Ancon, Republic of Panama

6: Energy and Resources Group, University of California, Berkeley, CA USA

7: Atmospheric Sciences and Global Change Division, Pacific Northwest National Laboratory, Richland, WA, USA

8: School of Biological Sciences, Washington State University, Pullman, WA, USA

Corresponding author: Chonggang Xu (cxu@lanl.gov)

**Abstract**: Vegetation plays a key role in the global carbon cycle and thus is an important component within Earth system models (ESMs) that project future climate. Many ESMs are adopting methods to resolve plant size and ecosystem disturbance history using vegetation demographic models. These models make it feasible to conduct more realistic simulation of processes that control vegetation dynamics. Meanwhile, increasing understanding of the processes governing plant water use, and ecosystem responses to drought in particular, has led to the adoption of dynamic plant water transport (i.e., hydrodynamic) schemes within ESMs. However, the impact of plant hydraulic trait variation in trait-diverse tropical forests is understudied. In this study, we report on a sensitivity analysis of an existing hydrodynamics (HYDRO) model that is updated and incorporated into the Functionally Assembled Terrestrial Ecosystem simulator (FATES). The size and canopy structured representation within FATES is able to simulate how plant size and hydraulic traits affect vegetation dynamics and carbon/water fluxes. To better understand this new model system and its functionality in tropical forest systems in particular, we conducted a global parameter sensitivity analysis at Barro Colorado Island, Panama. We assembled 942 observations of plant hydraulic traits on 306 tropical plant species for stomata, leaves, stems, and roots, and determined the best-fit statistical distribution for each trait, which was used in model parameter sampling to assess the parametric sensitivity. We showed that, for simulated leaf water potential and loss of hydraulic conductivity across different plant organs, the four most important traits were associated with xylem conduit taper (buffers increasing hydraulic resistance with tree height), stomatal sensitivity to leaf water potential, maximum stem hydraulic conductivity, and the partitioning of total hydraulic resistance above vs. belowground. Our analysis of individual ensemble members revealed that trees at a high risk of hydraulic failure and potential tree mortality generally have higher conduit taper, maximum xylem conductivity, stomatal sensitivity to leaf

48 water potential, and lower resistance to xylem embolism for stem and transporting roots. We
49 expect that our results will provide guidance on future modeling studies using plant hydrodynamic
50 models to predict the forest responses to droughts, and future field campaigns that aim to better
51 parameterize plant hydrodynamic models.

52

## 1. Introduction

Tropical forests play a critical role in regulating regional and global climates (Bonan, 2008). Under ongoing and future climate change, they are subjected to substantial risks of climate extremes such as drought and heat waves (Mcdowell et al., 2018). Studies have already shown that tropical forests were experiencing elevated tree mortality rates due to mega droughts related to ENSO events. For example, the 2015–16 El Niño led to the death of an estimated 2.5 ± 0.3 billion stems in the Lower Tapajós river basin of the Amazon and the associated carbon loss had not yet been compensated by new plant growth three years after the event (Berenguer et al., 2021). Such extreme climate events are projected to increase in frequency and intensity under a warming future (Seneviratne et al., 2021). A statistical analysis based on the projection of 13 ESMs under a high greenhouse emission scenario showed that the frequency of extreme droughts as defined by rhizosphere soil moisture (occurring once every 50 years) could increase by a factor of nearly four and this increase would have a disproportionate impact on tropical forests (Xu et al., 2019). The high species diversity found in tropical forests may result in increased resilience to climate extremes, based on the demonstrated resilience of temperate forests in relationship to trait diversity (Anderegg et al., 2018). However, due to limited data to parameterize and constrain models for tropical forests, there is a large uncertainty in our predictive understanding of how tropical forests will respond to these climate extremes (Bonal et al., 2016). This tropical forest uncertainty is a key source of the global uncertainty in projections of land carbon fluxes and future climates (Arora et al., 2020).

Earth System Models (ESMs) have been developed to project future changes to the coupled climate and biosphere system. Typically, 'big leaf' approximations of vegetation with no explicit presentation of tree size and canopy structure have been used to predict the impact of vegetation on carbon and water cycles. These models do not represent the fundamental elements of vegetation dynamics including growth, mortality, competition, and their response to disturbances. In the last decade, many ESMs have incorporated vegetation demographic models (VDMs) that represent plant size, canopy structure and disturbance histories, with the goal of better representing the competitive dynamics among different size classes of trees and plant functional types in response to climate and disturbances (Fisher et al., 2018). Most of these VDMs can differentiate plants' light, water and carbon use strategies and can thus represent some part of the functional diversity of tropical forests (Massoud et al., 2019; Koven et al., 2020).

Following the 'big leaf' model, water limitation on plant gas exchange in these VDMs is generally calculated based on three factors: 1) soil water potential; 2) root distribution; and 3) water potential for stomata openness and closure, all of which differ by plant functional types (Koven et al., 2020). While these soil-moisture-dependent water limitation functions are able to capture trait diversity in leaf-level stomatal behaviors, they fail to capture plant functional diversity in many other observable plant hydraulic traits, such as xylem capacitance, water potentials for loss of xylem hydraulic conductivity, stem hydraulic safety margin, and turgor loss point (Hochberg et al., 2018). Many studies have shown that plant hydraulic traits play an important role in plant responses to droughts (Su et al., 2022; Anderegg et al., 2016), which could shape the landscape distribution of plant functional types (Kunert et al., 2021). In view of this limitation, plant hydrodynamic models have been developed with the aim of better

simulating forest response to droughts (Powell et al., 2018; Christoffersen et al., 2016; Xu et al., 2016; Kennedy et al., 2019; Mcdowell et al., 2013). These models not only incorporate hydraulic functional diversity, but also mechanistically simulate the risk of plant mortality due to hydraulic functional failure, as a result of an inability to move water in the xylem due to embolism in conduits (Hammond et al., 2019).

One key challenge for these plant hydrodynamic models is that they have many more parameters than simple water limitation functions based on soil water potentials and thus inherently possess more uncertainty in the model parameterization and subsequent simulations. In this study, we describe the implementation of a hydrodynamic scheme within DOE-sponsored functionally assembled terrestrial ecosystem simulator (FATES) (Koven et al. 2020), and assess this new configuration with two goals: 1) quantify the parametric sensitivity of different hydraulic traits in determining plant hydrodynamics; and 2) identify key hydraulic traits that are important for predicting the risk of mortality due to hydraulic failure. We expect that our results will provide guidance on model parameterization for future modeling studies using plant hydrodynamic models to predict tropical forest response to droughts, and future field campaigns that aim to collect observational data that can be used to better parameterize and benchmark plant hydrodynamic models.

## 2. Methodology

### 2.1. Model description

We use FATES, a VDM that is coupled within the Energy Exascale Earth System Model (E3SM) (Caldwell et al., 2019). FATES represents size-structured groups of plants (cohorts) and successional trajectory-based patches using the ecosystem demography approach (Fisher et al., 2015; Moorcroft et al., 2001). FATES simulates growth by integrating photosynthesis

across different leaf layers for each cohort. FATES allocates this photosynthate to different tissues including leaves, fine and coarse roots, and stem, based on the allometry of different plant functional types, as well as a carbon storage pool (Fisher et al., 2015). Mortality within FATES is simulated by several mechanisms, including carbon starvation caused by depletion of the storage pool, hydraulic function failure, as well as impact mortality during disturbance, fire, logging, freezing, age-related and 'background' constant turnover (Fisher et al., 2015; Huang et al., 2020; Fisher et al., 2010; Needham et al., 2020).

### 2.1.1. Plant Hydrodynamics

The default (non-hydrodynamic) FATES model contains a simplistic algorithm that approximates plant hydraulic failure thresholds based on soil water potential. An important feature of the plant hydrodynamic scheme (HYDRO), which explicitly simulates water flow from the soil through leaves to the atmosphere, is that it enables direct representation of percent loss of conductance as a predictor of hydraulic failure mortality rates. FATES-HYDRO is based on the hydrodynamic model implemented in the Traits-based Forest Simulator (TFS) (Christoffersen et al., 2016) and the features most relevant to the present analysis are summarized below. The model approximates water transport in a single vertical dimension, approximating the canopy as a single leaf layer at the top of a beam, according to the Shinozaki pipe model (Shinozaki et al., 1964) in which the hydraulic path length from the trunk base to each leaf is assumed constant. Following the 'porous media' approach, the model simulates the water transport across four main organs (leaves, stem- trunk/branches, transporting roots, and absorbing roots) and different rhizosphere shells (Fig. 1). Resistors connect the different compartments.

The water flow is calculated based on water pressure gradients across different compartments (rhizosphere, absorbing roots, transporting roots, stem, and leaf). Specifically, flow between compartment $i$ and $i + 1$ ($Q_i$) is given by,

$$Q_i = - K_i \Delta h_i, \quad (1)$$

where $K_i$ is the total conductance (kg MPa$^{-1}$ s$^{-1}$) at the boundary of compartments $i$ and $i + 1$ and $\Delta h_i$ is the total matric potential difference between the compartments,

$$\Delta h_i = \rho_w g(z_i - z_{i+1}) + (\psi_i - \psi_{i+1}), \quad (2)$$

where $z_i$ is compartment elevation difference above (+) or below (-) the soil surface (m), $\rho_w$ is the density of water ($10^3$ kg m$^{-3}$), $g$ is acceleration due to gravity (9.8 m s$^{-2}$), and $\psi_i$ is tissue or soil matric water potential (MPa). $K_i$ is treated here as the product of a maximum boundary conductance between compartments $i$ and $i + 1$ ($K_{max,i}$), and the fractional maximum hydraulic conductance of the upstream compartments ($FMC_i$ or $FMC_{i+1}$), which is a function of the tissue water potential as follows,

$$FMC_i = \left[1 + \left(\frac{\psi_i}{P_{50,x}}\right)^{a_x}\right]^{-1} \quad , \quad (3)$$

where $\psi_i$ is the compartmental water potential, $P_{50,x}$ is the water potential at 50% loss of maximum conductivity for different plant tissues ( absorbing root, transporting root, stem), $a_x$ is the corresponding vulnerability curve shape parameter, with a larger number indicating a steeper reduction of conductivity in response to more negative water potentials (Choat et al., 2012). The maximum percentage loss of conductivity (PLC) across different organs [i.e., $PLC_i$ =100 (1-$FMC_i$) ] is used to measure the risk of tree mortality ($M_{hf}$) resulting from hydraulic failure as follows,

$$M_{hf} = M_{hf,base} \frac{\max(0,\ PLC_{max,organ} - PLC_c)}{100 - PLC_c}, \quad (4)$$

where $PLC_c$ is the critical percentage loss of conductivity with risk of mortality, $PLC_{max,organ}$ is the maximum percentage loss of conductivity across different organs, $M_{hf,base}$ is the baseline mortality rate [fraction/year] when percentage loss of conductivity exceeds $PLC_c$. In this version of model, we assume that xylem cavitation can fully recover as long as the trees do not die.

The previous version of this model (TFS-Hydro) presented water in terms of relative water content (RWC; g $H_2O$ $g^{-1}$ $H_2O$ at saturation) in line with most empirical work on plant water relations. While the underlying equations remain unchanged, here we present water in terms of volumetric water content ($\theta$; $m^3$ $H_2O$ $m^{-3}$ plant tissue), since this what is accounted by the model and is consistent with what is tracked in the soil as well. The two quantities are related via the equation RWC = $\theta/\theta_{sat}$, where $\theta_{sat}$ indicates saturated volumetric water content. The water potential for tissue $x$ [$\psi_x$] is related to $\theta_x$ (the PV curve) following three stages of water tissue drainage as follows (Tyree and Yang, 1990; Bartlett et al., 2012),

$$\psi_x = \begin{cases} \psi_{0,x} + m_{cap}\left(\frac{\theta_x}{\theta_{sat,x}} - 1\right) & \theta_{ft} < \theta_x \leq \theta_{sat,x} \\ \psi_{sol}(\theta_x) + \psi_p(\theta_x) & \theta_{tlp,x} < \theta_x \leq \theta_{ft,x} \\ \psi_{sol}(\theta_x) & \theta_{r,x} < \theta_x \leq \theta_{tlp,x} \end{cases} \quad (5)$$

Stage one applies to stem and roots only and represents the water draw from capillary reserves (embolized conduits or airspaces in wood) when wood water content is in between full turgor ($\theta_{ft} = RWC_{ft}\,\theta_{sat,x}$) and saturation ($\theta_{sat,x}$) and only represents a small fraction of the total PV curve. It is linear with constant slope $m_{cap}$ = 11.3 MPa $m^3$ $m^{-3}$ and $RWC_{ft}$ = 0.958 as estimated from sapwood PV curves on 28 tropical and subtropical species (Christoffersen et al. 2016). $RWC_{ft}$ is assumed to be 1.0 in leaves. Xylem water potential is assumed zero at full saturation. The second stage is between full turgor ($\theta_{ft,x}$) and the turgor loss point ($\theta_{tlp,x}$),

when the xylem water potential is in balance with solute ($\psi_{sol}[\theta_x]$) and pressure water potential ($\psi_p[\theta_x]$) of living cells. The third stage is after the turgor loss point ($\theta_{tlp,x}$), but above the point of residual water content ($\theta_{r,x} = RWC_{r,x}\,\theta_{sat,x}$) where the water potential is only a function of the solute water potential. $RWC_{r,x}$ is synonymous with the apoplastic fraction (Bartlett et al. 2012).

The solute water potential is given as,

$$\psi_{sol}[\theta_x] = \frac{\pi_0(\theta_{sat,x}RWC_{ft} - \theta_{r,x})}{(\theta_x - \theta_{r,x})}, \quad (6)$$

where $\pi_0$ is the tissue osmotic potential at full turgor. The pressure potential is calculated as follows,

$$\psi_p[\theta_x] = -|\pi_0| + \varepsilon\frac{(\theta_x - \theta_{sat,x}RWC_{ft})}{(\theta_{sat,x}RWC_{ft} - \theta_{r,x})}\ , \quad (7)$$

where ε is the bulk elastic modulus (MPa).

The realized conductivity of the above ground portion of the plant per unit of leaf area ($K_{l,max,tree,ag}$) is calculated based on xylem hydraulic conductivity at petiole ($k_{s,max,petiole}$), aboveground tree height (H, meters), and a xylem taper factor ($X_{tap}$) as follows,

$$K_{l,max,tree,ag} = \frac{k_{s,max,petiole}}{H(\frac{A_l}{A_s})}X_{tap}, \quad (8)$$

where $k_{s,max,petiole}$ is scaled from the xylem conductivity measured from the branch ($k_{s,max}$) (Christoffersen et al., 2016). $\frac{A_l}{A_s}$ [i.e., la2sa in Table 1] is the ratio of leaf area ($A_l$) to sapwood area ($A_s$). $X_{tap}$ is the xylem taper factor representing the ratio of aboveground xylem conductance with taper to that without, which for intermediate values of conduit taper (*p_taper* = 1/6; see below) represents a factor increase in total conductance of 23–50 for trees of heights 10–30 meters (Christoffersen et al., 2016). Savage et al. (2010) highlighted how opposing

selective forces will both increase hydraulic conductance by the tapering of conduit radii (*p_taper* > 0) while at the same time protect against embolism by minimizing conduit taper (no taper implies *p_taper* = 0). They defined *p_taper* as the exponent on an external branching parameter (2 daughter branches per parent branch in their model) that sets the degree of internal branching of xylem conduits (and thus the tapering of conduit radii as well) and, using a fractal network model, derived an effective exponent $q$ that describes how aboveground conductance increases with tree size. $q$ is a monotonically increasing and saturating function of the taper exponent $p$ (see Fig 2b of Savage et al. 2010); we used this relationship to estimate $q$, and thus $X_{tap}$ in eq. (8) as

$$X_{tap} = \left[\frac{r_{base}}{r_{petiole}}\right]^{q_{tap}-q_{notap}}, \quad (9)$$

where $r_{base}$ and $r_{petiole}$ are the trunk and petiole radii, respectively. The ratio $r_{base}/r_{petiole}$ is related to tree height following the fractal tree model of Savage et al. (2010) (see equations S12-S13 in Christoffersen et al. 2016).

Eq. (8) only gives the aboveground component of whole-plant conductance. In the absence of a simple first-principles approach to estimating the belowground component, we estimate the total tree maximum conductance (above- and belowground components) as

$$K_{max,tree,total} = R_{frac,stem} K_{max,tree,ag}, \quad (10)$$

where $R_{frac,stem}$ is the fraction of total resistance that is aboveground.

Stomatal conductance [$g_s$, μmol $m^{-2}$ $s^{-1}$] is simulated through a modified Ball-Berry equation,

$$g_s = g_0 + g_1 \frac{A_n}{C_s/P_{atm}} h_s \quad , \quad (11)$$

where $g_1$ is the stomatal conductance slope in response to environmental condition changes, $g_0$ is the minimum (cuticular) stomatal conductance (μmol $m^{-2}$ $s^{-1}$), $C_s$ is the leaf surface $CO_2$ partial pressure (Pa), $P_{atm}$ is the atmospheric pressure (Pa), $h_s$ is the leaf surface humidity, and $A_n$ is leaf net photosynthesis rate (μmol $CO_2$ $m^{-2}$ $s^{-1}$). Stomatal conductance (i.e., both $g_0$ and $g_1$) is further modified by a plant water stress factor, $\beta$, calculated as

$$\beta = [1 - \left(\frac{\psi_{leaf}}{P_{50,gs}}\right)^{a_{gs}}]^{-1}, \quad (12)$$

where $\psi_{leaf}$ is the leaf water potential, $P_{50,gs}$ is leaf water potential at 50% loss of maximum stomatal conductance, and $a_{gs}$ is the stomatal vulnerability shape parameter.

The total fine root surface area affects the amount of water a plant can take up through its influence on rhizosphere conductance and is determined by both the specific root length (srl) and absorbing root radius (*rs2*). Specifically, the model has a specified number of soil shells (5 in this study) around fine root surfaces and the conductance between soil shell *k+1* and *k* , $K_{shell,k}$, is calculated as,

$$K_{shell,k} = K_s \frac{\pi\, l_{aroot,common}}{\ln(r_{k+1}/r_k)}, \quad (13)$$

where $r_k$ is the mean radi of *k*th shell, $l_{aroot,common}$ is the total length of absorbing roots calculated as a product of total fine root biomass and specific root length (*srl*). $K_s$ is set to be the conductance for soil ($K_{soil}$) when *k*>1. For *k* = 1,

$$K_s = \frac{1}{\frac{1}{K_{soil}} + \frac{1}{K_{root\_soil}}}, \quad (14)$$

where $K_{root\_soil}$ is the conductance between fine root surface and soil. An update to the TFS-Hydro approach is to make this conductance direction-specific, in view that water loss rate from root could be substantially lower than water uptake rate either through osmatic regulation (Dichio et al., 2006) or by lacunae caused by rupture of cortical cells (North and Nobel, 1992)

during drought. It is determined by either the maximum uptake of water per unit of absorbing root surface area ($k_{r1,max,}$ kg $m^{-1}$ $s^{-1}$ $MPa^{-1}$) when root water potential is more negative than adjacent rhizosphere soil water potential, or the maximum root water loss rate per unit surface area ($k_{r2,max}$, kg $m^{-1}$ $s^{-1}$ $MPa^{-1}$) when rhizosphere water potential becomes more negative than root water potential, which may occur, for example, in frozen soils or in very dry soil layers (Schmidhalter, 1997).

The plant hydrodynamic representation and numerical solver scheme within FATES-HYDRO follows the 1-D solver laid out by Christoffersen et al. (2016), which is the default solver in FATES-HYDRO and used in this study. The model also has an option of a 2-D solver, which is slower and detailed by Fang et al. (2022) and Lambert et al. (2022). The equations are solved for tissue water content at a 30 minutes time step. We made a few modifications to accommodate multiple soil layers and improve the numerical stability. First, to accommodate the multiple-soil layers, we sequentially solve the Richards' equation for each individual soil layer, with each layer-specific solution proportional to each layer's contribution to the total root-soil conductance. Second, to improve the numerical stability, we now linearly interpolate the pressure/volume curve beyond the residual and saturated tissue water content to avoid the rare cases of overshooting in the numerical scheme under very dry or wet conditions. See the Supplementary Information [HYDRO_DESCRIPTION.pdf] for further details of the implementation.

#### 2.1.2. Non-hydrodynamics processes

FATES-HYDRO can be coupled to different host land models (HLMs) including the E3SM land model (ELM) (Caldwell et al., 2019) or the Community Terrestrial Systems Model (CTSM) (Lawrence et al., 2019). In this study, the model is coupled to ELM. In this section,

we layout the key non-hydrodynamic processes in the FATES or the ELM for a better understanding of parameter importance in the results.

Canopy radiative transfer is calculated using a multi-layer scheme based on the iterative Norman radiation scheme (Norman, 1979). Leaf and stem area is binned into a matrix of canopy layer, leaf layer and plant functional types. Reflectance, absorption, and transmittance are calculated for each leaf layer. Between canopy layers, light streams are averaged between plant functional types (PFTs), such that all PFTs in understory layers receive equal radiation on their top leaf layer. Fractional absorption of visible and near infra-red light is calculated separately for direct and diffuse light. For the direct stream, transmitted and reflected light is converted into diffuse fluxes. In FATES, the absorbed PAR is used to calculate photosynthesis rates for each of the canopy layer x leaf layer x PFT bins, after which rates across layers are re-aggregated into cohort level carbon fluxes. Please see the Supplementary file in Fisher et al. (2015) for details.

The energy balance is handled by the host land model. In this study, it is based on the land component of DOE's Exascale Energy Earth System Model (E3SM). The E3SM land model (ELM) is based on the Community Land Model 4.5 (Oleson, 2013). Specifically, in ELM, the average canopy temperature is calculated based on the energy balance of latent heat, sensible heat, and absorbed radiation as determined by the radiative transfer model. The latent heat is determined by the transpiration, which is determined by the vapor pressure deficit from inside of leaf to the air, canopy stomatal conductance, and boundary layer conductance. FATES calculated mean canopy stomatal conductance averaged across different cohorts, which is fed to ELM to calculate the energy balance. The Newton-Raphson numerical scheme is used to solve for the canopy temperature.

All aspects of soil water balance (infiltration, water transfer among soil layers, and drainage) happen at the 'column' scale at 30-min time steps and are handled within the Host Land Model (see Oleson et al. 2013 for a detailed description of hydrology in CLM4.5, the parent model of ELM). FATES-HYDRO handles soil water operations at the patch and cohort scales. It simulates root water uptake and changes in plant water potential from roots to leaves based on current time step transpiration. The belowground conductance for each soil layer is weighted by root biomass with an exponential vertical distribution. Sections 2 and 3 in the Supplement of this manuscript provide full details on boundary conditions, sequence of operations among HYDRO and the HLM, downscaling of soil moisture to rhizosphere shells, and downscaling of transpiration from the patch to individual scale.

**2.2. Sensitivity analysis**

We identified 35 parameters for the FATES-HYDRO model to conduct the parametric sensitivity analysis (Table 1). To estimate the parameter distributions, we started with published meta-analyses (Christoffersen et al., 2016; Choat et al., 2012; Bartlett et al., 2012; Bartlett et al., 2014; Bartlett et al., 2016; Klein, 2014) and supplemented them with select new data from individual studies. Focal data were tissue- or individual-level hydraulic traits spanning water transport and embolism resistance, tissue water storage and retention (PV curve traits), hydraulic architecture (i.e., leaf area to sapwood area ratio), stomatal responses to dehydration, and fine root traits (Table 1). For each dataset, we standardized taxonomic names using the TNRS package in R (Boyle et al., 2013). This allowed us to join datasets together based on species, averaging multiple observations per species if necessary, resulting in a species-specific sparse matrix of all hydraulic traits for all databases and individual studies that

we compiled. This pantropical hydraulic trait dataset is included in the Supporting Information [traits_master_trop.csv].

This trait dataset consisted of anywhere from 1 - 323 observations for each trait, where each observation corresponds to a different species (multiple observations for the same species are first averaged; see above). Before fitting distributions to these data, some traits were first transformed to be positive (e.g., P50) or normalized within [0, 1] when upper and lower bounds were well-defined (Table 1). Then, for each trait separately, we used the fitdistr package in R to estimate best-fit parameters for uniform, beta, normal, lognormal, and gamma statistical distributions in order to estimate central tendencies and spread for each trait. The distribution with the largest log likelihood and best-fit parameters are given in Table 1. Each model simulation consisted of a single PFT: all trees (across all cohort sizes and patches) had the same traits.

We augmented observations with extratropical data to increase sample size for traits with less than three tropics-specific observations. When trait data observations were not present, we used a uniform distribution bounded on our best estimate of the theoretical range (Table 1). As there is limited data on roots, we used the same distribution as that for branches if data were lacking. Because our goal is to understand the model behaviors as determined by different hydraulic traits, we assumed independence among traits. As we focused on the hydraulic traits in this study, we used non-hydraulic trait values based on an optimal set of parameters that best fit observed water and carbon fluxes in a set of FATES simulations run without hydrodynamics (Koven et al., 2020).

We used the Fourier Amplitude Sensitivity Test (FAST) to assess the relative importance of parameters in determining the variance of model outputs (Xu and Gertner, 2011a). The main idea of FAST is to assign periodic signals in the sampled parameter values and use Fourier transformation to identify the signals in the outputs. Sampled parameter values are based on Latin hypercube sampling from the fitted statistical distributions (see previous section for more details). We ran 1000 ensemble simulations of the FATES-Hydro to derive model outputs of water potential and fraction of maximum conductivity. For each ensemble simulation, each plant hydraulic trait was assigned with a random draw from each trait's distribution, and the samples for different traits are randomly combined to sample the observed plant hydraulic trait space for sensitivity analysis.

We used the Uncertainty Analysis and Sensitivity Analysis (UASA) tool (https://sites.google.com/site/xuchongang/uasatoolbox) to estimate the parametric sensitivity index, which is calculated based on the ratio of the partial variance in the model output attributed to a specific parameter to the total variables in the model output. For details, please refer to Xu and Gertner (2011a). We ran the model with 1000 ensemble members, in view that an order of 100 times effective important number of parameters, which we estimate to be ~10, is needed to achieve reasonable precision (Xu and Gertner, 2011b).

### 2.3. Study area

In this study, we used Barro Colorado Island (BCI), Panama, as our test site to evaluate model behavior. We chose BCI because it has moderately strong dry and wet seasons that allow us to assess the hydrodynamics under different levels of water availability. Moreover, extensive field campaigns in recent years have provided comprehensive data needed for model

parameterization, initialization and climate drivers. Finally, we also leverage prior FATES studies of non-hydraulic parameters at BCI (Koven et al., 2020).

BCI has an annual mean temperature of 26.3ºC and an annual mean precipitation of 2656 mm with a strong seasonal precipitation signal. The dry season lasts from January to April, with a mean precipitation of 228mm, while the wet season lasts from May-December with a mean precipitation of 2428mm (Paton, 2020). In this study, we used hourly in-situ climate data from 2008-2016 to drive the model. To run the model to equilibrium (in terms of soil moisture content) takes 5-6 years, thus we choose February of 2016 as the target for analysis of dry season hydrodynamics and August of 2016 as the target for analysis of wet season hydrodynamics.

### 2.4. Model setup

In this study, as our focus is on the plant hydrodynamics, we used the static stand structure mode of FATES that turns off the processes of competition, growth and mortality, to instead hold the ecosystem structure constant. This reduced-complexity configuration (Fisher and Koven, 2020) thus exercises only the primarily fast-timescale-processes of photosynthesis, transpiration, water transport, and plant hydrodynamics (i.e., change in hydraulic conductivity, water storage, and water potentials in plant tissues). By using static stand structure mode, as in Chitra-Tarak et al. (2021), we isolate hydraulic trait controls on simulated hydrodynamics and avoid confounding, and potentially biased, feedbacks from resulting changes in forest structure. Using static stand structure mode also means that we do not need to spin up vegetation state, thus reducing the simulation time. The forest stand structure, consisting of tree size and composition for each patch, is initialized based on forest inventory data collected in 2015 (http://ctfs.si.edu/webatlas/datasets/bci/). As the majority of species in BCI are

evergreen broad leaf trees, we ran the model with one PFT with different hydraulic traits (Table 1) to assess their impact on the hydrodynamically relevant outputs including water potentials and fraction of maximum conductivity for different plant organs including absorbing root, transporting root, stem, and leaves.

One key benefit of utilizing a hydrodynamic model is its ability to simulate the risk of hydraulic failure by considering the loss of conductivity in various plant organs. As FATES model was ran on the static stand mode, we did not specifically simulate the tree mortality resulting from the hydraulic failure as shown in Eq. (4). Instead, we used the maximum of loss of conductance across the continuum of plant nodes [i.e., $PLC_{max,organ}$ in eq. (4)] to assess the hydraulic failure risk. If $PLC_{max,organ}$ reaches critical threshold $PLC_c$, which is set to 50% (Adams et al., 2017), trees are assumed to be faced with a high risk of mortality. Using the ensemble simulations, we also aim to identify the most vulnerable plant organs and the critical parameters that influence the likelihood of hydraulic failure. The HDYRO model only considers the stem node (Fig. 1) without explicitly simulating the branch. In this analysis, we calculated the branch vulnerability by using the PLC curve of xylem and the leaf water potential, which approximates the water potential at the tip of the branch. The model does not explicitly consider xylary or extraxylary resistance within and outside the leaf midrib.

FATES simulates the carbon and water fluxes for different size classes of trees. The forest has 137 cohorts with diameters ranging from 10 cm to >2 meters and height ranging from 1 to 38 meters (see Fig. S1 for size distributions). Because large trees experience more fluctuations in environmental conditions in the canopy and higher risk of mortality due to drought (Bennett et al., 2015), we focused on hydrodynamic behaviors for large trees with diameter at breast

height (DBH) more than 60 cm; however, for comparison, we also derived the sensitivity for smaller trees with DBH less than 60 cm.

## 3. Results

Our results showed that the simulated ranges across the ensemble of leaf water potential (Fig. 2) and loss of conductivity (Fig. 3) are large. For leaf water potential of large trees with diameter > 60 cm, the 95% percentile ranges are from -5 MPa to -0.5 MPa and -3 MPa to -0.5 MPa for February (dry) and August (wet) 2016, respectively. Correspondingly, the fraction of maximum stem hydraulic conductivity is much higher during August compared to February (Fig. 3); however, in both months, the modeled range spans almost the full range of between 0 and 1. For smaller trees with diameter less than 60 cm, our results show that smaller tree experienced less negative water potential (Fig. S2 and Fig. 2) and lower loss of hydraulic conductivity (Fig. S3 and Fig. 3).

Based on the FAST sensitivity indices (i.e., the variance in model output contributed by different parameters), the key parameters that control the water potentials of different plant organs (leaf, stem and root) for large trees (diameter >60 cm) include the taper exponent for hydraulic conductivity (*p_taper*), the water potential leading to 50% loss of stomatal conductance (*p50_gs*), maximum hydraulic conductivity for the stem (*kmax_node_stem*), and the fraction of total hydraulic resistance in the above ground section (*rfrac_stem*), in decreasing order (Fig. 4). For the fractional loss of conductivity, the most important parameter is the water potential leading to 50% loss of hydraulic conductance ($P_{50}$) for the corresponding organs (Fig. 5). Other important parameters are similar to those for simulated water potentials. Notably, the organ-specific $P_{50}$ values are more important for the dry month (February) compared to the wet month (August). For the wet month of August, *p_taper* is the dominant parameter

controlling the pre-dawn and midday loss of hydraulic conductivity, while organ-specific $P_{50}$ parameters are the second most important. For smaller trees with diameter less than 60 cm, the corresponding parametric sensitivity patterns are similar to those of larger trees (Fig. S4 and Fig. S5); however, compared to larger trees, the parametric sensitivity of *p_taper* for simulated leaf water potential becomes lower for smaller trees (Fig. 4 and Fig. S4).

In terms of the risk of hydraulic failure, out of the 1000 ensemble members, ~40% of the simulations for February and ~60% of simulation for August suggest that branches are the most vulnerable plant organ, based on highest loss of conductivity across the continuum from root to branch (Fig. 6). For the dry month of February, roots are at greater risk in comparison to the wet season. If we consider the loss of conductivity more than 50% for February 2016 as a threshold for a high risk of mortality (Adams et al., 2017), then 53% of ensemble simulations reach this threshold. The key parameters affecting the risk of mortality, as measured by percentage difference in parameter values for ensemble members reaching 50% loss of conductivity or not, include the water potential leading to 50% loss of conductance for stomata (*p50_gs*), stem (*p50_node_stem*), and transporting roots (*p50_node_troot*), maximum hydraulic conductivity of stem (*kmax_node_stem*), and the taper exponent (*p_taper*) (Fig. 7). Ensemble members with high risk of mortality generally have a higher *p_taper* and *kmax_node_stem*, less negative *p50_gs*, and less negative p50 for stem and transporting roots (Fig. 8).

## 4. Discussion

Our analysis showed the importance of key plant hydraulic traits in simulating plant water potential and risk of hydraulic failure. This analysis identifies these parameters as potential targets of either model calibration or targeted measurement campaigns to achieve realistic

simulations. In our sensitivity analysis, the most influential parameter for both water potential and loss of conductivity is the tapering of the radius of conduit with increasing plant height (*p_taper*). As *p_taper* increases, the conduit radius increases from the top of the tree to its base. According to Hagen-Poiseuille's equation, this increases the theoretical maximum total conductance. Low values of *p_taper* thus limit the adverse effects of tree height by increasing *k_max* along the whole continuum and reducing the soil-to-leaf water potential needed to maintain transpiration. Our inference is that *p_taper* represents an overarching property of plant architecture that influences the relative effect of each of the other traits related to hydraulic safety and efficiency (Olson et al., 2021). The xylem architecture as determined by *p_taper* parameter could change in response to age and development stages (Rodriguez-Zaccaro et al., 2019), which is not considered in this study. Future studies evaluating the importance of this change to hydraulic functions could be useful to guide size-dependent growth and mortality. Another dimension of the hydraulic architecture with a critical role in determining both water potential and loss of conductivity, though to a much lesser degree, was the fraction of total tree resistance that is belowground (i.e., of the entire transporting and absorbing root system; 1- *rfrac_stem*). Generally, a plant will match the growth of its trunk and crown to maintain a degree of equilibrium in aboveground resistance as the distance water needs to travel increases (Yang and Tyree, 1993). In this study, due to the lack of data on the belowground resistance, we assigned a quite large range for this trait, which could be impacted by many factors such as belowground root biomass, root network architecture, and interactions between roots, fungi and bacteria (Poudel et al., 2021; Bhagat et al., 2021).

The second most sensitive parameter in determining loss of conductance was the leaf water potential at 50% loss of stomatal conductance (*p50_gs*). This parameter controls the water loss

476 rate from leaves, with a less negative value providing protection from hydraulic failure during
477 water-limited periods. The *p50_gs* trait has been shown to play a key role in tree survival
478 during severe droughts (Breshears et al., 2009; Rowland et al., 2015). The ability to withstand
479 lower leaf water potentials is also a key indicator of sapling and seedling survival during
480 drought and determines species distribution across a moisture gradient (Kursar et al., 2009).
481 There may be a trade-off between drought tolerance (with a lower *p50_gs*) and drought
482 avoidance (a less negative *p50_gs* but with a high capacitance; the amount of water released
483 from reserves as leaf water potential declines), a crucial aspect in determining species drought
484 resistance (Pineda-Garcia et al., 2013). Additionally, loss of conductivity was sensitive to the
485 water potential at 50% loss of max conductivity within the stem (*p50_stem*) as it can largely
486 affect the whole plant conductance and thus the water supply to the leaves. *p50_stem*
487 negatively correlates with wood density and may be a marker of the trade-off between
488 hydraulic efficiency and safety within the stem (Chen et al., 2009; Manzoni et al., 2013);
489 however, other studies have shown that this trade-off is weak (Gleason et al., 2016). Liang et
490 al (2019) showed that the strength of this trade-off could be dependent on specie's drought
491 strategies.

492 Leaf water potential and loss of conductance were both sensitive to the maximum xylem
493 conductivity in the stem (*kmax_node_stem*). Higher maximum conductivity represents greater
494 xylem efficiency, which in the absence of drought or light limitations would result in greater
495 potential photosynthesis and less negative water potentials (Gleason et al., 2016). However,
496 xylem with higher *kmax_node_stem* could be more vulnerable to embolism as water potential
497 declines (Sperry and Love, 2015). In tropical rainforests, species with higher conductivity per
498 unit leaf area generally are less desiccation-tolerant, and thus exhibit higher mortality rates

(Kursar et al., 2009). Low *kmax_node_stem* along with high leaf-to-sapwood area ratio (*la2sa*) also represents a vulnerability to reduced conductance which increases with height (Christoffersen et al., 2016).

Traits with lower order of impacts on water potential modulate the amount of stored water available during drought. The bulk modulus of elasticity in the root (*epsil_node_aroot*) together with root saturated water content determines the amount of water available from cellular storage between complete hydration and loss of turgor (Powell et al., 2017). This represents the ability of the roots to continually supply water to the rest of the plant as drought occurs. It also represents an investment in cellular structure, which may be an additional indicator of adaptations with non-hydraulic origin. The residual water content in the stem (*resid_node_stem*) determines the minimum amount of water xylem will hold and thus impact the amount of water storage plant can use during drought as well (Bartlett et al. 2012). In this study, we made the assumption that the traits are independent of each other, in order to understand the hydrodynamic behaviors of FATES-HYDRO for different hydraulic traits based on a single PFT. Understanding the trade-offs between these traits is crucial for determining the competition among different PFTs. Future studies would greatly benefit from assessing the significance of these trade-offs to predict vegetation dynamics under future climate change.

In contrast to the majority of hydraulic traits in the model, conduit taper, the fraction of total resistance belowground, and the leaf to sapwood area ratio are whole-plant hydraulic traits. Our analysis highlights the importance of whole-plant hydraulic traits such as conduit taper relative to tissue-level hydraulic traits for a range of plant hydraulic functions, including whole-plant conductance and hydraulic failure risks. An important area for future work is to

better constrain and understand the consequences of intra- and interspecific variation in these whole-plant hydraulic traits in tropical forests. Our choice of the range of variation in the conduit taper exponent came from a study on temperate species, and was broad, encompassing the entire range of observed values in that study (Savage et al. 2010). Further, we estimated the effects of variation in the taper exponent on whole-plant conductance conditional on trees following a simple set of optimality assumptions (space-filling, area-conserving, and self-similar branching network structure). However, in practice, such assumptions are often not met (Smith et al., 2014). Therefore, it is possible that the model sensitivity to xylem taper in terms of whole-plant hydraulic function are overestimated. Nevertheless, our study highlights the importance of better constraining this parameter as well as further experimentation with alternate model structures to better account for non-optimal trees in tropical forests.

The sensitivity of vegetation to drought stress and hydraulic-failure-induced mortality is of paramount importance for understanding how ecosystems may respond to shifting temperature and rainfall patterns under a changing climate (Mcdowell et al., 2022). We recognize that parametric sensitivity could be different for different sites depending on climate driver, soil moisture and vegetation types. However, we expect the main parameter of importance could be useful to guide model calibration to select the candidate parameters for different sites. As understanding of plant hydrodynamics increases, linking model predictions to observable plant traits has emerged as a promising means of constraining predictions of ecosystem resilience. Such traits are challenging and costly to measure in the field and thus resources must be directed carefully when planning measurement campaigns. The identified parameters in this study could provide guidance on the limited measurement we could target in the field.

## 5. Acknowledgment

This research was supported as part of the Next Generation Ecosystem Experiments-Tropics, funded by the U.S. Department of Energy, Office of Science, Office of Biological and Environmental Research. RF acknowledges funding by the European Union's Horizon 2020 (H2020) research and innovation program under Grant Agreement No. 101003536 (ESM2025 – Earth System Models for the Future) and 821003 (4C, Climate-Carbon Interactions in the Coming Century).

## 6. CODE and Data Availability

The FATES-HYDRO code is available from https://doi.org/10.5281/zenodo.7686333. The traits data are in the supplementary file [traits_master_trop.csv].

## 7. Supplement Information

Three supplementary file are included. The HYDRO_DESCRIPTION.pdf provide the summary of the hydrodynamic implementation that is different from Christoffersen et al. (2016). The traits_master_trop.csv file include all the hydraulic traits we assembled for the tropical region. The supplementary_figure.pdf provides additional figures for the main text.

## 8. Author contribution

CX and BC designed the sensitivity analysis experiments. BC collected the data and fitted the trait distributions. CX conducted the analysis and drafted the manuscript. BC, CX, RF, RN and CK designed the implementation of HYDRO codes. BC implemented the majority of HYDRO codes with code improvement made by CX and RN. ZR conducted the ensemble model simulations. MS provided the leaf cuticular conductance data. NM, CK and LK provided guidance on the sensitivity analysis, code development and trait data synthesis. All authors contributed to manuscript writing by providing edits and suggestions.

## 9. Competing interests

The contact author has declared that none of the authors has any competing interests.

570

571 **Figures**

572

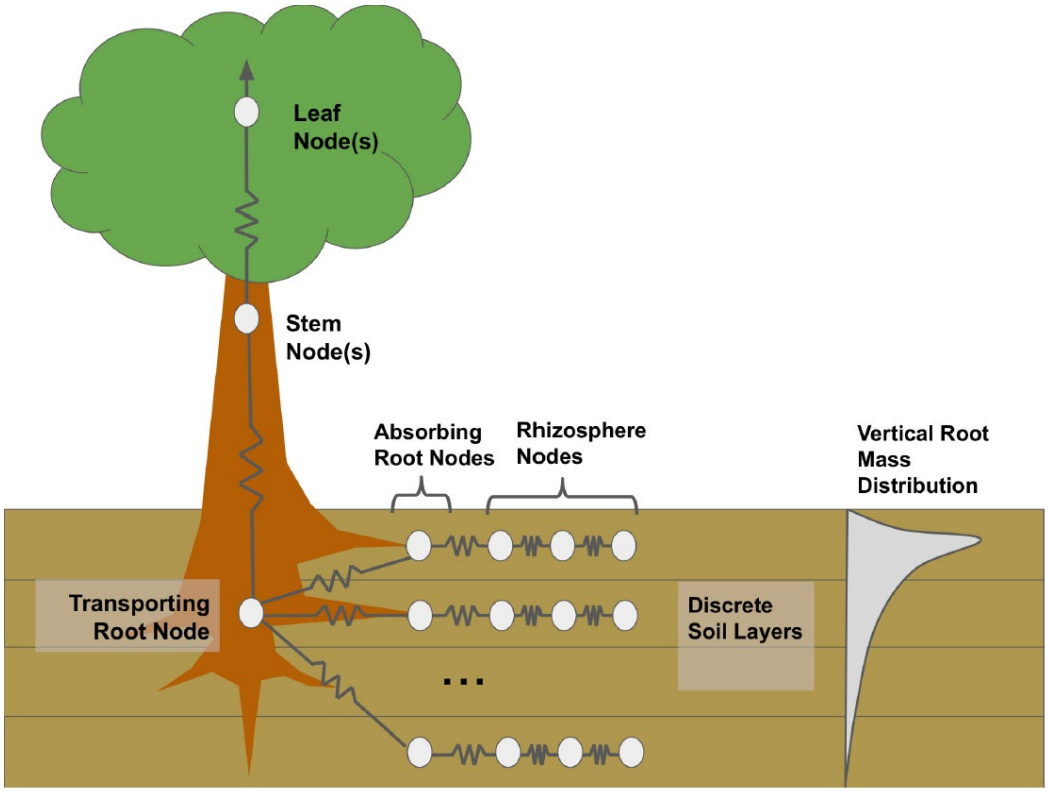


573

574 **Figure 1: Diagram of FATES-HYDO with simulation of rhizosphere shell, absorbing roots, transporting roots, stem and**

575 **leaves.** The model is solved for different soil layers with different root distributions.

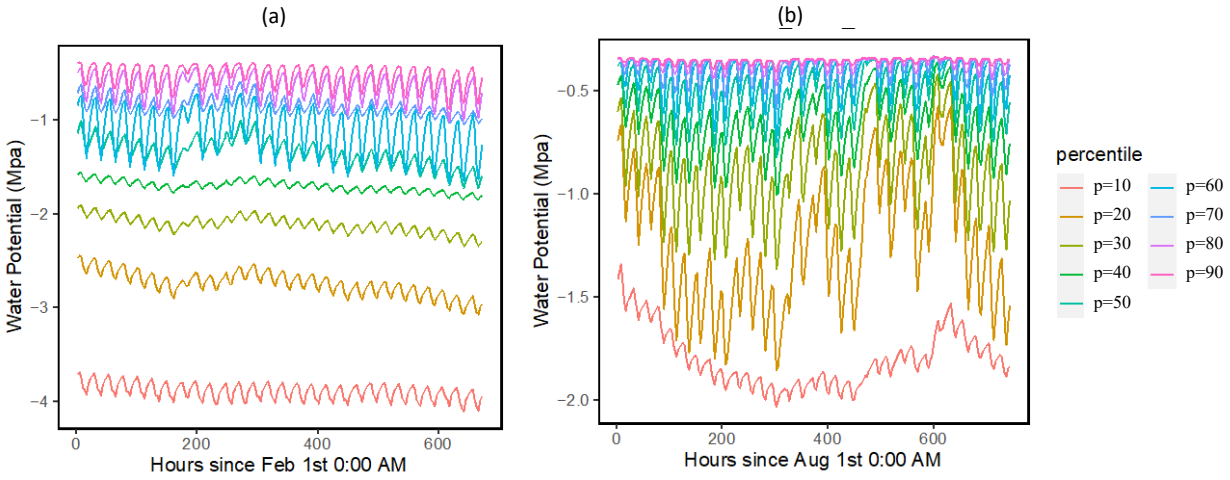


**Figure 2: Simulated ranges of leaf water potential for February (a) and August (a), 2016 for trees with DBH > 60cm.** The percentiles are calculated based on the monthly mean values of leaf water potentials for the 1000 ensemble simulations.

583

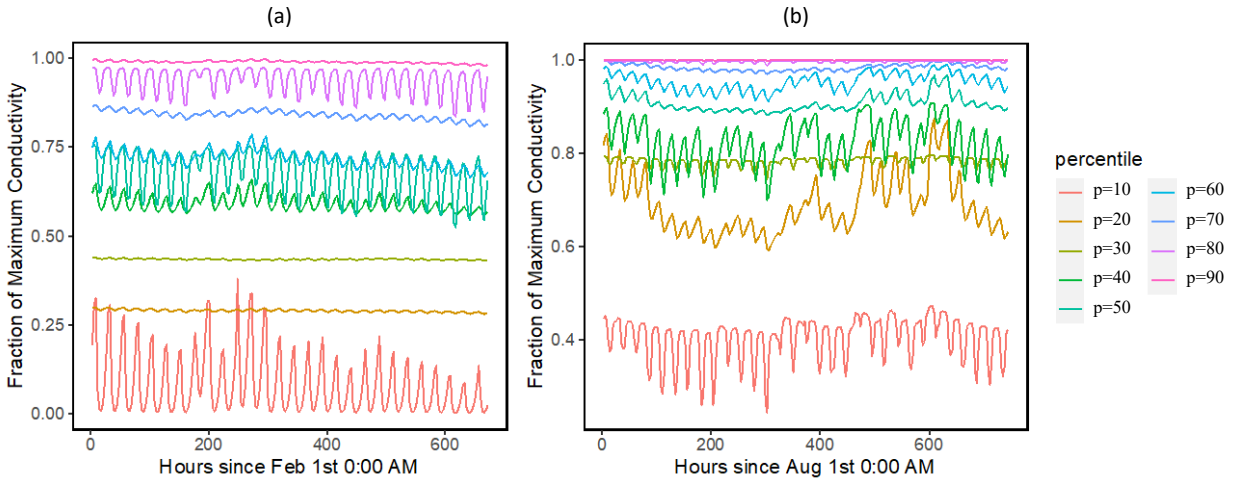


584

585 **Figure 3: Simulated ranges of fraction of maximum hydraulic conductivity of stem for February (a) and August (a), 2016**

586 **for trees with DBH > 60cm**. The percentiles are calculated based on the monthly mean values of leaf water potentials for the

587 1000 ensemble simulations.

588

589

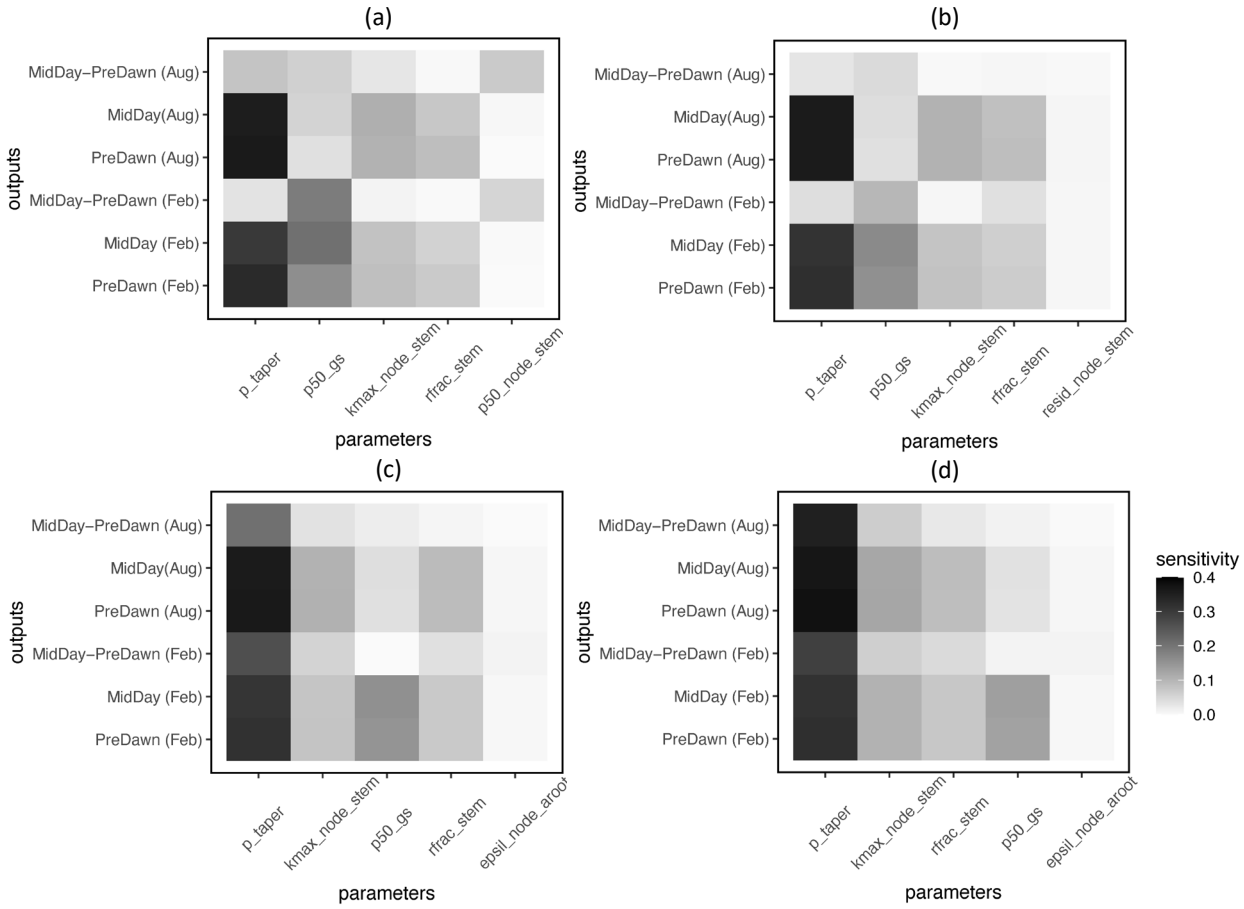


**Figure 4: Key parameters that control simulated water potentials for leaf (a), stem (b), transporting root (c) and absorbing root (d), for trees with DBH > 60cm.** The sensitivity value refers to the proportion of total model output variance contributed by a specific parameter (0-1). See Table 1 for the explanation of the parameters.

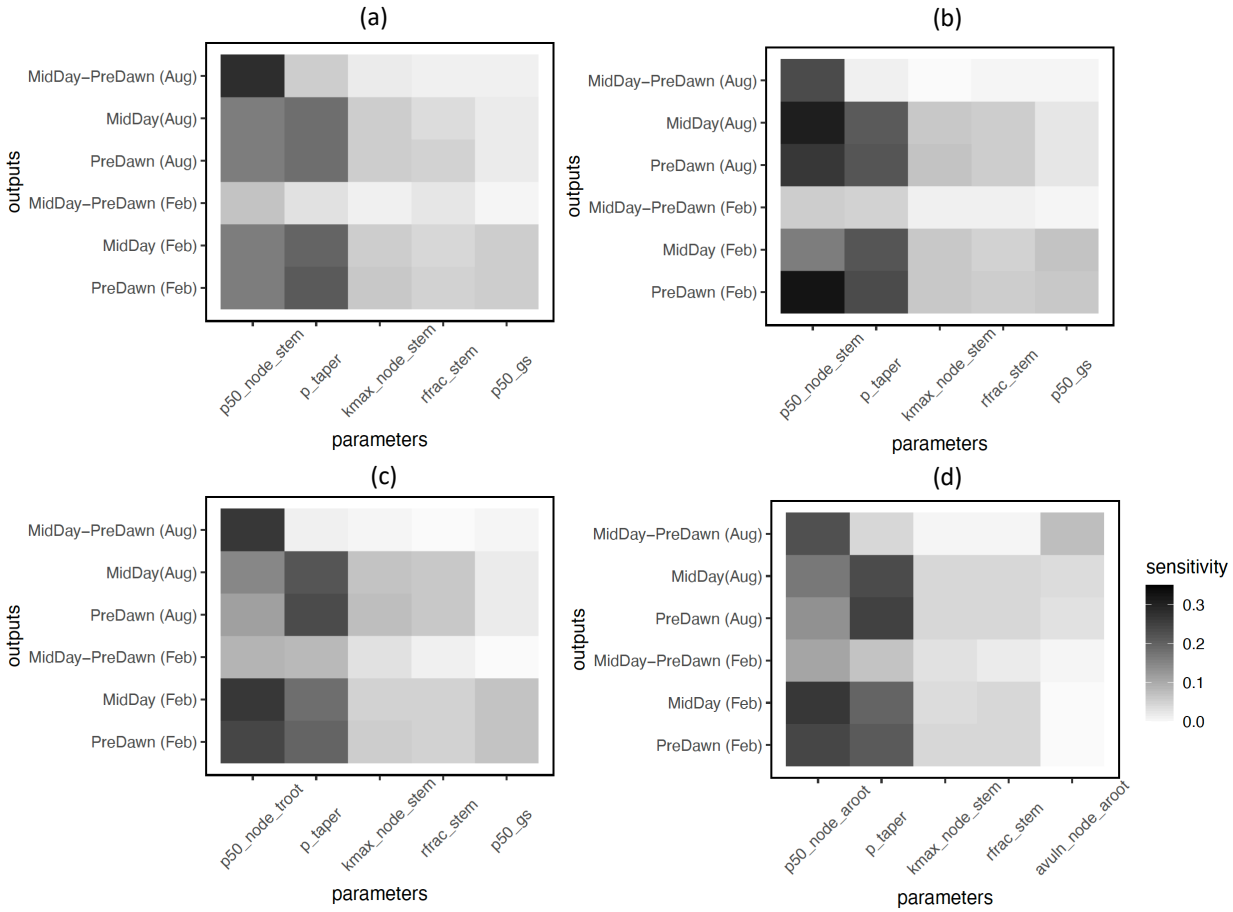


595

596

597 **Figure 5: Key parameters that control simulated loss of conductivity for branch (a), stem (b), transporting root (c) and**
598 **absorbing root (d), for trees with DBH > 60cm.** The sensitivity value refers to the proportion of total model output variance
599 contributed by a specific parameter. See Table 1 for the explanation of the parameters. See Table 1 for the description of
600 parameters.

601

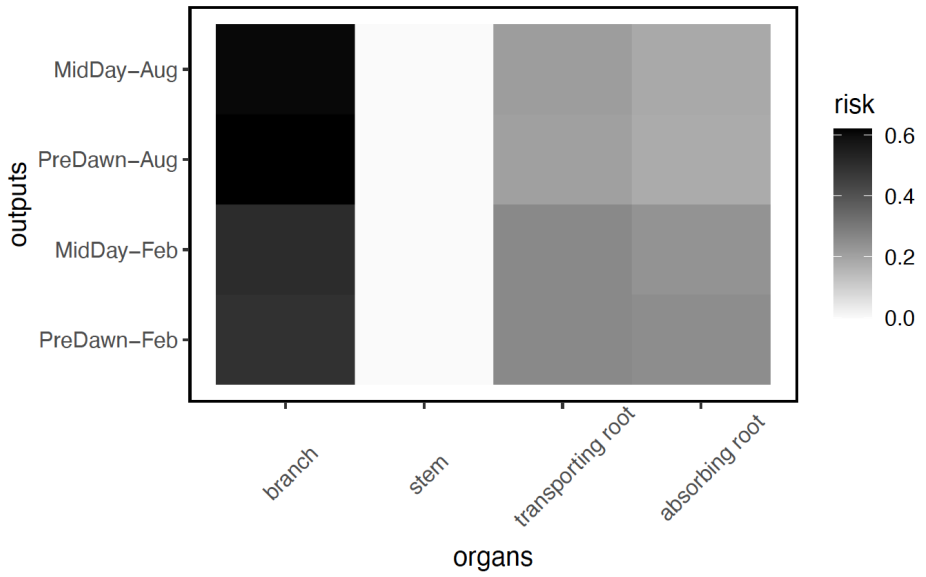


602

603 **Figure 6: Risk on the continuum for hydraulic failure as measured by percentage of total number of simulations with**
604 **highest loss of conductivity for a specific organ (branch, stem, transporting root and absorbing root), for trees with DBH**
605 **> 60cm.** As the model does not specifically simulate the branch, we calculated the risk of loss of conductivity based on the leaf
606 water potential and hydraulic vulnerability curve from xylem.

607

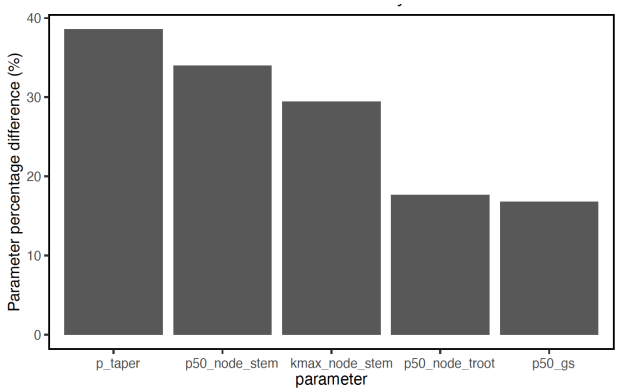


**Figure 7: Mean trait percentage difference for model ensemble simulations with loss of hydraulic conductivity larger than 50% and ensemble simulations with loss of hydraulic conductivity less than 50%, for trees with DBH > 60cm.** See Table 1 for the description of parameters.

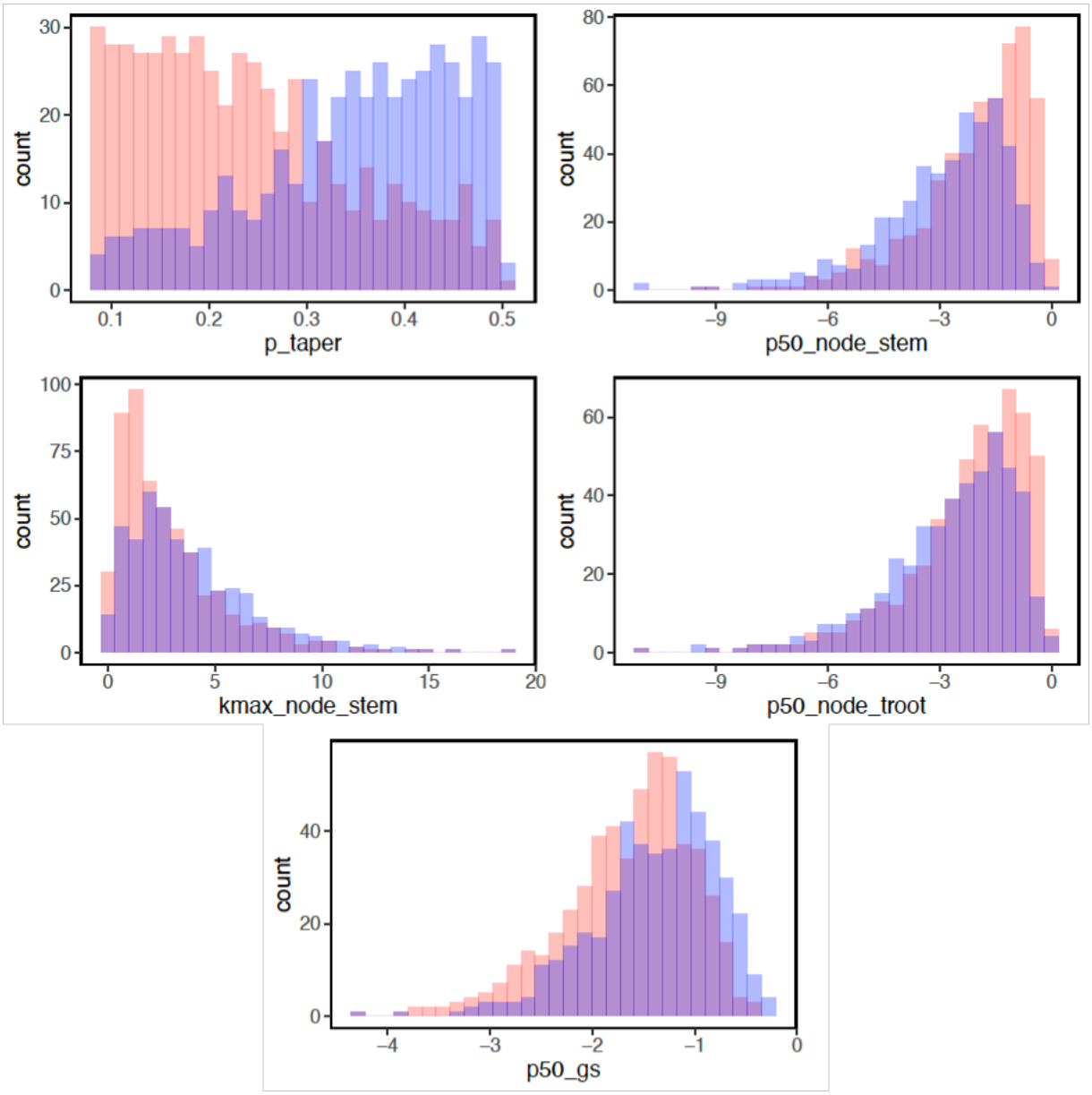


**Figure 8: Parameter difference for ensemble members with risk of mortality, for trees with DBH > 60cm.** Blue bars indicate parameter values with lower mortality risk (<50% loss of hydraulic conductivity). Red bars indicate parameter values with higher mortality risk (>= 50% loss of hydraulic conductivity) and purple bars indicate parameter values stacked from transparent red/blue bars. See Table 1 for the description of parameters.

624
625 Table 1 Hydraulic parameters considered in the sensitivity analysis

| PARAMETER (EQUATION NUMBER)[1] | SYMBOL[2] | UNITS | DISTRIBUTION[3] | SOURCES& NOTES |
|---|---|---|---|---|
| **Pressure-Volume (PV) curve (water content – water potential relationship)** | | | | |
| saturated water content (thetas_node_leaf, thetas_node_stem, thetas_node_troot, thetas_node_aroot) (Eq. 5) | $\theta_{sat,x}$ | $cm^3\ cm^{-3}$ | Leaf: Beta (9.69, 6.20)<br>Stem: Beta (12.67, 7.4626)<br>TRoot and ARoot: Beta (22.98, 5.29) | Christoffersen et al. (2016)<br>Iversen et al. (2017)<br>Wright et al. (2010)<br>Roderick et al. (1999)<br>Sack et al. (2003)<br>Binks et al. (2016) |
| turgor loss point (tlp_node_leaf, tlp_node_stem, tlp_node_troot, tlp_node_aroot) (Eq. 5) | $\pi_{tlp,x}$ | MPa | $\pi_{tlp} = (\pi_0\ \boldsymbol{\varepsilon})\ /(\pi_0 + \boldsymbol{\varepsilon})$ | Bartlett et al. (2012)<br>Christoffersen et al. (2016) |
| osmotic potential at full turgor (pinot_node_leaf, pinot_node_stem, pinot_node_troot, pinot_node_aroot) (Eq. 6) | $\pi_{0,x}$ | MPa | Leaf: G [9.8,6.26], Stem, TRoot, ARoot: LN [0.32,0.39] | Bartlett et al. (2012, 2014, 2016)<br>Christoffersen et al. (2016) |
| bulk elastic modulus (epsil_node_leaf, epsil_node_stem, epsil_node_troot, epsil_node_aroot) (Eq. 7) | $\boldsymbol{\varepsilon}_x$ | MPa | Leaf: G (4.07, 4.12)<br>Stem, TRoot and ARoot: G [3.57, 3.84] | Bartlett et al. (2012, 2014)<br>Christoffersen et al. (2016) |
| residual water fraction (resid_node_leaf, resid_node_stem, resid_node_troot, resid_node_aroot) (Eq. 5) | $RWC_{r,x}$ | unitless | Leaf: B [2.14,4.10]<br>Stem, TRoot and ARoot: B [2.71, 4.53] | Bartlett et al. (2012, 2014)<br>Christoffersen et al. (2016) |
| **Vulnerability Curve (water potential – hydraulic conductivity relationship)** | | | | |
| water potential at 50% loss of max conductivity (p50_node_stem, p50_node_troot, p50_node_aroot) (Eq. 3) | $P_{50,x}$ | MPa | Stem, TRoot and ARoot: G [2.07, 1.18] | Choat et al. (2012) |
| vulnerability curve shape parameter (avuln_node_stem, avuln_troot, avuln_node_aroot) (Eq. 3) | $a_x$ | unitless | Stem, TRoot and ARoot: LN [0.82,0.66] | Choat et al. (2012) |
| xylem conductivity per unit sapwood area (kmax_node_stem) (Eq. 8) | $k_{s,max}$ | $kg\ m^{-1}\ s^{-1}\ MPa^{-1}$ | G [1.41, 2.37] | Choat et al. (2012) |

| | | | | |
|---|---|---|---|---|
| **Leaf hydraulics** | | | | |
| leaf water potential at 50% loss of max gs (p50_gs) (Eq. 12) | $P_{50,gs}$ | MPa | G [5.73, 0.27] | Klein (2014) |
| stomatal vulnerability shape parameter(avuln_gs) (Eq. 12) | $a_{gs}$ | unitless | $a_{gs}$= -2.406 P50,gs (-P50,gs) $^{-1.25}$ | Christoffersen et al. (2016) |
| Leaf cuticular conductivity (k0_leaf) (Eq. 11) | $g_0$ | umol $m^{-2}s^{-1}$ | LN [1.04, 0.84] | Slot et al. (2021) |
| **Plant Hydraulic Architecture** | | | | |
| Xylem taper exponent for sapwood (p_taper) (Eq. 9) | $p$ | (-) | U (0.08, 0.5) | Savage et al. (2010) |
| Leaf area to sapwood area ratio (la2sa) (Eq. 8) | $\frac{A_l}{A_s}$ | (-) | LN (-0.48, 0.77) | Choat et al. (2012) |
| **Root hydraulic Traits** | | | | |
| specific root length (*srl*) (Eq. 13) | $srl$ | m $g^{-1}$ | G [1.70, 35.31] | Iversen et al. (2017) |
| absorbing root radius (*rs2*) (Eq. 13) | $r$ | mm | LN [-1.91, 0.79] | Iversen et al. (2017) |
| fraction of total tree resistance that is aboveground (*rfrac_stem*) (Eq. 10) | $R_{frac,stem}$ | Unitless | U [0.1,0.7] | This study; empirical |
| root-soil interface conductivity per unit surface area ($K_{r1}$) (Eq. 14) | $k_{r1,max}$ | kg $m^{-1}$ $s^{-1}$ $MPa^{-1}$ | G [1.41, 2.37] | This study; empirically set the same as xylem conductivity |
| maximum root water loss rate ($K_{r2}$) (Eq. 14) | $k_{r2,max}$ | kg $m^{-1}$ $s^{-1}$ $MPa^{-1}$ | LN [-6.80, 0.92] | Wolfe (2020); Empirically set as 1/1000 bark water loss rate |

**Note:** 1: Several hydraulic parameters are used for different nodes of the plant including leaf, stem, transporting root (troot), and absorbing root (aroot). For better reference in the text, we provided a list of these parameters for specific nodes in the parenthesis; 2: Subscript *x* represents different tissue nodes in the model; 3:B-Beta distribution; U- Uniform distribution [lower limit, upper limit]; N-Gaussian distribution (mean, standard deviation); LN-Log Normal Distribution [mean, standard deviation]; G-Gamma distribution (lambda, scale); TRoot-Transporting root; ARoot-Absorbing root.

## Reference


Adams, H. D., Zeppel, M. J. B., Anderegg, W. R. L., Hartmann, H., Landhausser, S. M., Tissue, D. T., Huxman, T. E., Hudson, P. J., Franz, T. E., Allen, C. D., Anderegg, L. D. L., Barron-Gafford, G. A., Beerling, D. J., Breshears, D. D., Brodribb, T. J., Bugmann, H., Cobb, R. C., Collins, A. D., Dickman, L. T., Duan, H. L., Ewers, B. E., Galiano, L., Galvez, D. A., Garcia-Forner, N., Gaylord, M. L., Germino, M. J., Gessler, A., Hacke, U. G., Hakamada, R., Hector, A., Jenkins, M. W., Kane, J. M., Kolb, T. E., Law, D. J., Lewis, J. D., Limousin, J. M., Love, D. M., Macalady, A. K., Martinez-Vilalta, J., Mencuccini, M., Mitchell, P. J., Muss, J. D., O'Brien, M. J., O'Grady, A. P., Pangle, R. E., Pinkard, E. A., Piper, F. I., Plaut, J. A., Pockman, W. T., Quirk, J., Reinhardt, K., Ripullone, F., Ryan, M. G., Sala, A., Sevanto, S., Sperry, J. S., Vargas, R., Vennetier, M., Way, D. A., Xu, C. G., Yepez, E. A., and McDowell, N. G.: A multi-species synthesis of physiological mechanisms in drought-induced tree mortality, Nat Ecol Evol, 1, 1285-1291, 10.1038/s41559-017-0248-x, 2017.

Anderegg, W. R. L., Klein, T., Bartlett, M., Sack, L., Pellegrini, A. F. A., Choat, B., and Jansen, S.: Meta-analysis reveals that hydraulic traits explain cross-species patterns of drought-induced tree mortality across the globe, P Natl Acad Sci USA, 113, 5024-5029, 10.1073/pnas.1525678113, 2016.

Anderegg, W. R. L., Konings, A. G., Trugman, A. T., Yu, K. L., Bowling, D. R., Gabbitas, R., Karp, D. S., Pacala, S., Sperry, J. S., Sulman, B. N., and Zenes, N.: Hydraulic diversity of forests regulates ecosystem resilience during drought, Nature, 561, 538–541, 10.1038/s41586-018-0539-7, 2018.

Arora, V. K., Katavouta, A., Williams, R. G., Jones, C. D., Brovkin, V., Friedlingstein, P., Schwinger, J., Bopp, L., Boucher, O., Cadule, P., Chamberlain, M. A., Christian, J. R., Delire, C., Fisher, R. A., Hajima, T., Ilyina, T., Joetzjer, E., Kawamiya, M., Koven, C. D., Krasting, J. P., Law, R. M., Lawrence, D. M., Lenton, A., Lindsay, K., Pongratz, J., Raddatz, T., Seferian, R., Tachiiri, K., Tjiputra, J. F., Wiltshire, A., Wu, T. W., and Ziehn, T.: Carbon-concentration and carbon-climate feedbacks in CMIP6 models and their comparison to CMIP5 models, Biogeosciences, 17, 4173-4222, 10.5194/bg-17-4173-2020, 2020.

Bartlett, M. K., Scoffoni, C., and Sack, L.: The determinants of leaf turgor loss point and prediction of drought tolerance of species and biomes: a global meta-analysis, Ecol Lett, 15, 393-405, 10.1111/j.1461-0248.2012.01751.x, 2012.

Bartlett, M. K., Klein, T., Jansen, S., Choat, B., and Sack, L.: The correlations and sequence of plant stomatal, hydraulic, and wilting responses to drought, P Natl Acad Sci USA, 113, 13098-13103, 10.1073/pnas.1604088113, 2016.

Bartlett, M. K., Zhang, Y., Kreidler, N., Sun, S. W., Ardy, R., Cao, K. F., and Sack, L.: Global analysis of plasticity in turgor loss point, a key drought tolerance trait, Ecol Lett, 17, 1580-1590, 10.1111/ele.12374, 2014.

Bennett, A. C., McDowell, N. G., Allen, C. D., and Anderson-Teixeira, K. J.: Larger trees suffer most during drought in forests worldwide, Nat Plants, 1, Artn 15139 10.1038/Nplants.2015.139, 2015.

Berenguer, E., Lennox, G. D., Ferreira, J., Malhi, Y., Aragao, L. E. O. C., Barreto, J. R., Espirito-Santo, F. D., Figueiredo, A. E. S., Franca, F., Gardner, T. A., Joly, C. A., Palmeira, A. F., Quesada, C. A., Rossi, L. C., de Seixas, M. M. M., Smith, C. C., Withey, K., and Barlow, J.: Tracking the impacts of El Nino drought and fire in human-modified Amazonian forests, P Natl Acad Sci USA, 118, ARTN e2019377118: 10.1073/pnas.2019377118, 2021.

678 Bhagat, N., Raghav, M., Dubey, S., and Bedi, N.: Bacterial Exopolysaccharides: Insight into
679 Their Role in Plant Abiotic Stress Tolerance, J Microbiol Biotechn, 31, 1045-1059,
680 10.4014/jmb.2105.05009, 2021.
681 Binks, O., Meir, P., Rowland, L., da Costa, A. C. L., Vasconcelos, S. S., de Oliveira, A. A. R.,
682 Ferreira, L., Christoffersen, B., Nardini, A., and Mencuccini, M.: Plasticity in leaf-level water
683 relations of tropical rainforest trees in response to experimental drought, New Phytol, 211, 477-
684 488, 10.1111/nph.13927, 2016.
685 Bonal, D., Burban, B., Stahl, C., Wagner, F., and Herault, B.: The response of tropical rainforests
686 to drought-lessons from recent research and future prospects, Ann Forest Sci, 73, 27-44,
687 10.1007/s13595-015-0522-5, 2016.
688 Bonan, G. B.: Forests and climate change: Forcings, feedbacks, and the climate benefits of
689 forests, Science, 320, 1444-1449, 10.1126/science.1155121, 2008.
690 Boyle, B., Hopkins, N., Lu, Z., Raygoza Garay, J. A., Mozzherin, D., Rees, T., Matasci, N.,
691 Narro, M. L., Piel, W. H., and Mckay, S. J.: The taxonomic name resolution service: an online
692 tool for automated standardization of plant names, BMC bioinformatics, 14, 1-15, 2013.
693 Breshears, D. D., Myers, O. B., Meyer, C. W., Barnes, F. J., Zou, C. B., Allen, C. D., McDowell,
694 N. G., and Pockman, W. T.: Tree die-off in response to global change-type drought: mortality
695 insights from a decade of plant water potential measurements, Front Ecol Environ, 7, 185-189,
696 10.1890/080016, 2009.
697 Caldwell, P. M., Mametjanov, A., Tang, Q., Van Roekel, L. P., Golaz, J. C., Lin, W. Y., Bader,
698 D. C., Keen, N. D., Feng, Y., Jacob, R., Maltrud, M. E., Roberts, A. F., Taylor, M. A.,
699 Veneziani, M., Wang, H. L., Wolfe, J. D., Balaguru, K., Cameron-Smith, P., Dong, L., Klein, S.
700 A., Leung, L. R., Li, H. Y., Li, Q., Liu, X. H., Neale, R. B., Pinheiro, M., Qian, Y., Ullrich, P.
701 A., Xie, S. C., Yang, Y., Zhang, Y. Y., Zhang, K., and Zhou, T.: The DOE E3SM Coupled
702 Model Version 1: Description and Results at High Resolution, J Adv Model Earth Sy, 11, 4095-
703 4146, 10.1029/2019ms001870, 2019.
704 Chen, J. W., Zhang, Q., Li, X. S., and Cao, K. F.: Independence of stem and leaf hydraulic traits
705 in six Euphorbiaceae tree species with contrasting leaf phenology, Planta, 230, 459-468,
706 10.1007/s00425-009-0959-6, 2009.
707 Chitra-Tarak, R., Xu, C. G., Aguilar, S., Anderson-Teixeira, K. J., Chambers, J., Detto, M.,
708 Faybishenko, B., Fisher, R. A., Knox, R. G., Koven, C. D., Kueppers, L. M., Kunert, N., Kupers,
709 S. J., McDowell, N. G., Newman, B. D., Paton, S. R., Perez, R., Ruiz, L., Sack, L., Warren, J.
710 M., Wolfe, B. T., Wright, C., Wright, S. J., Zailaa, J., and McMahon, S. M.: Hydraulically-
711 vulnerable trees survive on deep-water access during droughts in a tropical forest, New Phytol,
712 231, 1798-1813, 10.1111/nph.17464, 2021.
713 Choat, B., Jansen, S., Brodribb, T. J., Cochard, H., Delzon, S., Bhaskar, R., Bucci, S. J., Feild, T.
714 S., Gleason, S. M., Hacke, U. G., Jacobsen, A. L., Lens, F., Maherali, H., Martinez-Vilalta, J.,
715 Mayr, S., Mencuccini, M., Mitchell, P. J., Nardini, A., Pittermann, J., Pratt, R. B., Sperry, J. S.,
716 Westoby, M., Wright, I. J., and Zanne, A. E.: Global convergence in the vulnerability of forests
717 to drought, Nature, 491, 752-+, 10.1038/nature11688, 2012.
718 Christoffersen, B. O., Gloor, M., Fauset, S., Fyllas, N. M., Galbraith, D. R., Baker, T. R., Kruijt,
719 B., Rowland, L., Fisher, R. A., Binks, O. J., Sevanto, S., Xu, C. G., Jansen, S., Choat, B.,
720 Mencuccini, M., McDowell, N. G., and Meir, P.: Linking hydraulic traits to tropical forest
721 function in a size-structured and trait-driven model (TFS v.1-Hydro), Geosci Model Dev, 9,
722 4227-4255, 10.5194/gmd-9-4227-2016, 2016.

723 Dichio, B., Xiloyannis, C., Sofo, A., and Montanaro, G.: Osmotic regulation in leaves and roots
724 of olive trees during a water deficit and rewatering, Tree Physiol, 26, 179-185, DOI
725 10.1093/treephys/26.2.179, 2006.
726 Fang, Y. L., Leung, L. R., Knox, R., Koven, C., and Bond-Lamberty, B.: Impact of the numerical
727 solution approach of a plant hydrodynamic model (v0.1) on vegetation dynamics, Geosci Model
728 Dev, 15, 6385-6398, 10.5194/gmd-15-6385-2022, 2022.
729 Fisher, R., McDowell, N., Purves, D., Moorcroft, P., Sitch, S., Cox, P., Huntingford, C., Meir, P.,
730 and Woodward, F. I.: Assessing uncertainties in a second-generation dynamic vegetation model
731 caused by ecological scale limitations, New Phytol, 187, 666-681, 10.1111/j.1469-
732 8137.2010.03340.x, 2010.
733 Fisher, R. A. and Koven, C. D.: Perspectives on the Future of Land Surface Models and the
734 Challenges of Representing Complex Terrestrial Systems, J Adv Model Earth Sy, 12, ARTN
735 e2018MS001453: 10.1029/2018MS001453, 2020.
736 Fisher, R. A., Muszala, S., Verteinstein, M., Lawrence, P., Xu, C., McDowell, N. G., Knox, R.
737 G., Koven, C., Holm, J., Rogers, B. M., Spessa, A., Lawrence, D., and Bonan, G.: Taking off the
738 training wheels: the properties of a dynamic vegetation model without climate envelopes,
739 CLM4.5(ED), Geosci Model Dev, 8, 3593-3619, 10.5194/gmd-8-3593-2015, 2015.
740 Fisher, R. A., Koven, C. D., Anderegg, W. R. L., Christoffersen, B. O., Dietze, M. C., Farrior, C.
741 E., Holm, J. A., Hurtt, G. C., Knox, R. G., Lawrence, P. J., Lichstein, J. W., Longo, M.,
742 Matheny, A. M., Medvigy, D., Muller-Landau, H. C., Powell, T. L., Serbin, S. P., Sato, H.,
743 Shuman, J. K., Smith, B., Trugman, A. T., Viskari, T., Verbeeck, H., Weng, E. S., Xu, C. G., Xu,
744 X. T., Zhang, T., and Moorcroft, P. R.: Vegetation demographics in Earth System Models: A
745 review of progress and priorities, Global Change Biol, 24, 35-54, 10.1111/gcb.13910, 2018.
746 Gleason, S. M., Westoby, M., Jansen, S., Choat, B., Hacke, U. G., Pratt, R. B., Bhaskar, R.,
747 Brodribb, T. J., Bucci, S. J., Cao, K. F., Cochard, H., Delzon, S., Domec, J. C., Fan, Z. X., Feild,
748 T. S., Jacobsen, A. L., Johnson, D. M., Lens, F., Maherali, H., Martinez-Vilalta, J., Mayr, S.,
749 McCulloh, K. A., Mencuccini, M., Mitchell, P. J., Morris, H., Nardini, A., Pittermann, J.,
750 Plavcova, L., Schreiber, S. G., Sperry, J. S., Wright, I. J., and Zanne, A. E.: Weak tradeoff
751 between xylem safety and xylem-specific hydraulic efficiency across the world's woody plant
752 species, New Phytol, 209, 123-136, 10.1111/nph.13646, 2016.
753 Hammond, W. M., Yu, K., Wilson, L. A., Will, R. E., Anderegg, W. R. L., and Adams, H. D.:
754 Dead or dying? Quantifying the point of no return from hydraulic failure in drought-induced tree
755 mortality, New Phytol, 223, 1834-1843, https://doi.org/10.1111/nph.15922, 2019.
756 Hochberg, U., Rockwell, F. E., Holbrook, N. M., and Cochard, H.: Iso/Anisohydry: A Plant-
757 Environment Interaction Rather Than a Simple Hydraulic Trait, Trends Plant Sci, 23, 112-120,
758 10.1016/j.tplants.2017.11.002, 2018.
759 Huang, M. Y., Xu, Y., Longo, M., Keller, M., Knox, R. G., Koven, C. D., and Fisher, R. A.:
760 Assessing impacts of selective logging on water, energy, and carbon budgets and ecosystem
761 dynamics in Amazon forests using the Functionally Assembled Terrestrial Ecosystem Simulator,
762 Biogeosciences, 17, 4999-5023, 10.5194/bg-17-4999-2020, 2020.
763 Iversen, C. M., McCormack, M. L., Powell, A. S., Blackwood, C. B., Freschet, G. T., Kattge, J.,
764 Roumet, C., Stover, D. B., Soudzilovskaia, N. A., Valverde-Barrantes, O. J., van Bodegom, P.
765 M., and Violle, C.: A global Fine-Root Ecology Database to address below-ground challenges in
766 plant ecology, New Phytol, 215, 15-26, 10.1111/nph.14486, 2017.

767 Kennedy, D., Swenson, S., Oleson, K. W., Lawrence, D. M., Fisher, R., da Costa, A. C. L., and
768 Gentine, P.: Implementing Plant Hydraulics in the Community Land Model, Version 5, J Adv
769 Model Earth Sy, 11, 485-513, 10.1029/2018ms001500, 2019.
770 Klein, T.: The variability of stomatal sensitivity to leaf water potential across tree species
771 indicates a continuum between isohydric and anisohydric behaviours, Funct Ecol, 28, 1313-
772 1320, 10.1111/1365-2435.12289, 2014.
773 Koven, C. D., Knox, R. G., Fisher, R. A., Chambers, J. Q., Christoffersen, B. O., Davies, S. J.,
774 Detto, M., Dietze, M. C., Faybishenko, B., Holm, J., Huang, M. Y., Kovenock, M., Kueppers, L.
775 M., Lemieux, G., Massoud, E., McDowel, N. G., Muller-Landau, H. C., Needham, J. F., Norby,
776 R. J., Powell, T., Rogers, A., Serbin, S. P., Shuman, J. K., Swann, A. L. S., Varadharajan, C.,
777 Walker, A. P., Wright, S. J., and Xu, C. G.: Benchmarking and parameter sensitivity of
778 physiological and vegetation dynamics using the Functionally Assembled Terrestrial Ecosystem
779 Simulator (FATES) at Barro Colorado Island, Panama, Biogeosciences, 17, 3017-3044,
780 10.5194/bg-17-3017-2020, 2020.
781 Kunert, N., Zailaa, J., Herrmann, V., Muller-Landau, H. C., Wright, S. J., Perez, R., McMahon,
782 S. M., Condit, R. C., Hubbell, S. P., Sack, L., Davies, S. J., and Anderson-Teixeira, K. J.: Leaf
783 turgor loss point shapes local and regional distributions of evergreen but not deciduous tropical
784 trees, New Phytol, 230, 485-496, 10.1111/nph.17187, 2021.
785 Kursar, T. A., Engelbrecht, B. M. J., Burke, A., Tyree, M. T., El Omari, B., and Giraldo, J. P.:
786 Tolerance to low leaf water status of tropical tree seedlings is related to drought performance and
787 distribution, Funct Ecol, 23, 93-102, 10.1111/j.1365-2435.2008.01483.x, 2009.
788 Lambert, M. S. A., Tang, H., Aas, K. S., Stordal, F., Fisher, R. A., Fang, Y. L., Ding, J. Y., and
789 Parmentier, F. J. W.: Inclusion of a cold hardening scheme to represent frost tolerance is
790 essential to model realistic plant hydraulics in the Arctic-boreal zone in CLM5.0-FATES-Hydro,
791 Geosci Model Dev, 15, 8809-8829, 10.5194/gmd-15-8809-2022, 2022.
792 Lawrence, D. M., Fisher, R. A., Koven, C. D., Oleson, K. W., Swenson, S. C., Bonan, G.,
793 Collier, N., Ghimire, B., van Kampenhout, L., Kennedy, D., Kluzek, E., Lawrence, P. J., Li, F.,
794 Li, H. Y., Lombardozzi, D., Riley, W. J., Sacks, W. J., Shi, M. J., Vertenstein, M., Wieder, W.
795 R., Xu, C. G., Ali, A. A., Badger, A. M., Bisht, G., van den Broeke, M., Brunke, M. A., Burns, S.
796 P., Buzan, J., Clark, M., Craig, A., Dahlin, K., Drewniak, B., Fisher, J. B., Flanner, M., Fox, A.
797 M., Gentine, P., Hoffman, F., Keppel-Aleks, G., Knox, R., Kumar, S., Lenaerts, J., Leung, L. R.,
798 Lipscomb, W. H., Lu, Y. Q., Pandey, A., Pelletier, J. D., Perket, J., Randerson, J. T., Ricciuto, D.
799 M., Sanderson, B. M., Slater, A., Subin, Z. M., Tang, J. Y., Thomas, R. Q., Martin, M. V., and
800 Zeng, X. B.: The Community Land Model Version 5: Description of New Features,
801 Benchmarking, and Impact of Forcing Uncertainty, J Adv Model Earth Sy, 11, 4245-4287,
802 10.1029/2018ms001583, 2019.
803 Manzoni, S., Vico, G., Katul, G., Palmroth, S., Jackson, R. B., and Porporato, A.: Hydraulic
804 limits on maximum plant transpiration and the emergence of the safety-efficiency trade-off, New
805 Phytol, 198, 169-178, 10.1111/nph.12126, 2013.
806 Massoud, E. C., Xu, C. G., Fisher, R. A., Knox, R. G., Walker, A. P., Serbin, S. P.,
807 Christoffersen, B. O., Holm, J. A., Kueppers, L. M., Ricciuto, D. M., Wei, L., Johnson, D. J.,
808 Chambers, J. Q., Koven, C. D., McDowell, N. G., and Vrugt, J. A.: Identification of key
809 parameters controlling demographically structured vegetation dynamics in a land surface model:
810 CLM4.5(FATES), Geosci Model Dev, 12, 4133-4164, 10.5194/gmd-12-4133-2019, 2019.
811 McDowell, N., Allen, C. D., Anderson-Teixeira, K., Brando, P., Brienen, R., Chambers, J.,
812 Christoffersen, B., Davies, S., Doughty, C., Duque, A., Espirito-Santo, F., Fisher, R., Fontes, C.

G., Galbraith, D., Goodsman, D., Grossiord, C., Hartmann, H., Holm, J., Johnson, D. J., Kassim, A., Keller, M., Koven, C., Kueppers, L., Kumagai, T., Malhi, Y., McMahon, S. M., Mencuccini, M., Meir, P., Moorcroft, P., Muller-Landau, H. C., Phillips, O. L., Powell, T., Sierra, C. A., Sperry, J., Warren, J., Xu, C. G., and Xu, X. T.: Drivers and mechanisms of tree mortality in moist tropical forests, New Phytol, 219, 851-869, 10.1111/nph.15027, 2018.
McDowell, N. G., Fisher, R. A., Xu, C. G., Domec, J. C., Holtta, T., Mackay, D. S., Sperry, J. S., Boutz, A., Dickman, L., Gehres, N., Limousin, J. M., Macalady, A., Martinez-Vilalta, J., Mencuccini, M., Plaut, J. A., Ogee, J., Pangle, R. E., Rasse, D. P., Ryan, M. G., Sevanto, S., Waring, R. H., Williams, A. P., Yepez, E. A., and Pockman, W. T.: Evaluating theories of drought-induced vegetation mortality using a multimodel-experiment framework, New Phytol, 200, 304-321, 10.1111/nph.12465, 2013.
McDowell, N. G., Sapes, G., Pivovaroff, A., Adams, H. D., Allen, C. D., Anderegg, W. R. L., Arend, M., Breshears, D. D., Brodribb, T., Choat, B., Cochard, H., De Caceres, M., De Kauwe, M. G., Grossiord, C., Hammond, W. M., Hartmann, H., Hoch, G., Kahmen, A., Klein, T., Mackay, D. S., Mantova, M., Martinez-Vilalta, J., Medlyn, B. E., Mencuccini, M., Nardini, A., Oliveira, R. S., Sala, A., Tissue, D. T., Torres-Ruiz, J. M., Trowbridge, A. M., Trugman, A. T., Wiley, E., and Xu, C. G.: Mechanisms of woody-plant mortality under rising drought, CO2 and vapour pressure deficit, Nat Rev Earth Env, 3, 294-308, 10.1038/s43017-022-00272-1, 2022.
Moorcroft, P. R., Hurtt, G. C., and Pacala, S. W.: A method for scaling vegetation dynamics: The ecosystem demography model (ED), Ecol Monogr, 71, 557-585, 10.1890/0012-9615(2001)071[0557:Amfsvd]2.0.Co;2, 2001.
Needham, J. F., Chambers, J., Fisher, R., Knox, R., and Koven, C. D.: Forest responses to simulated elevated CO2 under alternate hypotheses of size- and age-dependent mortality, Global Change Biol, 26, 5734-5753, 10.1111/gcb.15254, 2020.
Norman, J.: Modelling the complete crop canopy, in Modification of the Aerial Environment of Plants, Am. Soc. Agri. Eng. Monograph, 2, 249-277, 1979.
North, G. B. and Nobel, P. S.: Drought-Induced Changes in Hydraulic Conductivity and Structure in Roots of Ferocactus-Acanthodes and Opuntia-Ficus-Indica, New Phytol, 120, 9-19, DOI 10.1111/j.1469-8137.1992.tb01053.x, 1992.
Oleson, K. W., Lawrence, D. M., Bonan, G. B., Drewniak, B., Huang, M., Koven, C. D., Levis, S., Li, F., Riley, W. J., Subin, Z. M., Swenson, S. C., Thornton, P. E., Bozbiyik, A., Fisher, R., Heald, C. L., Kluzek, E., Lamarque, J.-F., Lawrence, P. J., Leung, L. R., Lipscomb, W., Muszala, S., Ricciuto, D. M., Sacks, W., Sun, Y., Tang, J., & Yang, Z.-L. : Technical description of version 4.5 of the Community Land Model (CLM) National Center for Atmospheric Research, Boulder, Colorado, USA.Tech. Rep. NCAR/TN-503+STR, 2013.
Olson, M. E., Anfodillo, T., Gleason, S. M., and McCulloh, K. A.: Tip-to-base xylem conduit widening as an adaptation: causes, consequences, and empirical priorities, New Phytol, 229, 1877-1893, 10.1111/nph.16961, 2021.
Paton, S.: Yearly Reports_Barro Colorado Island, Smithsonian Tropical Research Institute, https://doi.org/10.25573/data.11799111.v3, 2020.
Pineda-Garcia, F., Paz, H., and Meinzer, F. C.: Drought resistance in early and late secondary successional species from a tropical dry forest: the interplay between xylem resistance to embolism, sapwood water storage and leaf shedding, Plant Cell Environ, 36, 405-418, 10.1111/j.1365-3040.2012.02582.x, 2013.

857 Poudel, M., Mendes, R., Costa, L. A., Bueno, C. G., Meng, Y., Folimonova, S. Y., Garrett, K.
858 A., and Martins, S. J.: The role of plant-associated bacteria, fungi, and viruses in drought stress
859 mitigation, Frontiers in microbiology, 12, 3058, 2021.
860 Powell, T. L., Wheeler, J. K., de Oliveira, A. A. R., da Costa, A. C. L., Saleska, S. R., Meir, P.,
861 and Moorcroft, P. R.: Differences in xylem and leaf hydraulic traits explain differences in
862 drought tolerance among mature Amazon rainforest trees, Global Change Biol, 23, 4280-4293,
863 10.1111/gcb.13731, 2017.
864 Powell, T. L., Koven, C. D., Johnson, D. J., Faybishenko, B., Fisher, R. A., Knox, R. G.,
865 McDowell, N. G., Condit, R., Hubbell, S. P., Wright, S. J., Chambers, J. Q., and Kueppers, L.
866 M.: Variation in hydroclimate sustains tropical forest biomass and promotes functional diversity,
867 New Phytol, 219, 932-946, 10.1111/nph.15271, 2018.
868 Roderick, M. L., Berry, S. L., Saunders, A. R., and Noble, I. R.: On the relationship between the
869 composition, morphology and function of leaves, Funct Ecol, 13, 696-710, DOI 10.1046/j.1365-
870 2435.1999.00369.x, 1999.
871 Rodriguez-Zaccaro, F. D., Valdovinos-Ayala, J., Percolla, M. I., Venturas, M. D., Pratt, R. B.,
872 and Jacobsen, A. L.: Wood structure and function change with maturity: Age of the vascular
873 cambium is associated with xylem changes in current-year growth, Plant, Cell & Environment,
874 42, 1816-1831, https://doi.org/10.1111/pce.13528, 2019.
875 Rowland, L., da Costa, A. C. L., Galbraith, D. R., Oliveira, R. S., Binks, O. J., Oliveira, A. A. R.,
876 Pullen, A. M., Doughty, C. E., Metcalfe, D. B., Vasconcelos, S. S., Ferreira, L. V., Malhi, Y.,
877 Grace, J., Mencuccini, M., and Meir, P.: Death from drought in tropical forests is triggered by
878 hydraulics not carbon starvation, Nature, 528, 119-+, 10.1038/nature15539, 2015.
879 Sack, L., Cowan, P. D., Jaikumar, N., and Holbrook, N. M.: The 'hydrology' of leaves: co-
880 ordination of structure and function in temperate woody species, Plant Cell Environ, 26, 1343-
881 1356, DOI 10.1046/j.0016-8025.2003.01058.x, 2003.
882 Savage, V. M., Bentley, L. P., Enquist, B. J., Sperry, J. S., Smith, D. D., Reich, P. B., and von
883 Allmen, E. I.: Hydraulic trade-offs and space filling enable better predictions of vascular
884 structure and function in plants, P Natl Acad Sci USA, 107, 22722-22727,
885 10.1073/pnas.1012194108, 2010.
886 Schmidhalter, U.: The gradient between pre-dawn rhizoplane and bulk soil matric potentials, and
887 its relation to the pre-dawn root and leaf water potentials of four species, Plant, Cell &
888 Environment, 20, 953-960, https://doi.org/10.1046/j.1365-3040.1997.d01-136.x, 1997.
889 Seneviratne, S. I., Zhang, X., Adnan, M., Badi, W., Dereczynski, C., Luca, A. D., Ghosh, S.,
890 Iskandar, I., Kossin, J., Lewis, S., Otto, F., Pinto, I., Satoh, M., Vicente-Serrano, S. M., Wehner,
891 M., Zhou, B., and Allan, R.: Weather and climate extreme events in a changing climate, in:
892 Climate Change 2021: The Physical Science Basis: Working Group I contribution to the Sixth
893 Assessment Report of the Intergovernmental Panel on Climate Change, edited by: Masson-
894 Delmotte, V. P., Zhai, A., Pirani, S. L., and Connors, C., Cambridge University Press,
895 Cambridge, UK, 1513-1766, 2021.
896 Shinozaki, K., Yoda, K., Hozumi, K., and Kira, T.: A quantitative analysis of plant form-the pipe
897 model theory: I. Basic analyses, Japanese Journal of ecology, 14, 97-105, 1964.
898 Slot, M., Nardwattanawong, T., Hernandez, G. G., Bueno, A., Riederer, M., and Winter, K.:
899 Large differences in leaf cuticle conductance and its temperature response among 24 tropical tree
900 species from across a rainfall gradient, New Phytol, 232, 1618-1631, 10.1111/nph.17626, 2021.
901 Smith, D. D., Sperry, J. S., Enquist, B. J., Savage, V. M., McCulloh, K. A., and Bentley, L. P.:
902 Deviation from symmetrically self-similar branching in trees predicts altered hydraulics,

mechanics, light interception and metabolic scaling, New Phytol, 201, 217-229, 10.1111/nph.12487, 2014.
Sperry, J. S. and Love, D. M.: What plant hydraulics can tell us about responses to climate-change droughts, New Phytol, 207, 14-27, 10.1111/nph.13354, 2015.
Su, R., Liu, H., Wang, C., Zhang, H., and Cui, J.: Leaf turgor loss point is one of the best predictors of drought-induced tree mortality in tropical forest, Front Ecol Evol, 10, ARTN 974004: 10.3389/fevo.2022.974004, 2022.
Tyree, M. T. and Yang, S.: Water-storage capacity of Thuja, Tsuga and Acer stems measured by dehydration isotherms: the contribution of capillary water and cavitation, Planta, 182, 420-426, 1990.
Wei, L., Xu, C. G., Jansen, S., Zhou, H., Christoffersen, B. O., Pockman, W. T., Middleton, R. S., Marshall, J. D., and McDowell, N. G.: A heuristic classification of woody plants based on contrasting shade and drought strategies, Tree Physiol, 39, 767-781, 10.1093/treephys/tpy146, 2019.
Wolfe, B. T.: Bark water vapour conductance is associated with drought performance in tropical trees, Biol Letters, 16, ARTN 20200263: 10.1098/rsbl.2020.0263, 2020.
Wright, S. J., Kitajima, K., Kraft, N. J. B., Reich, P. B., Wright, I. J., Bunker, D. E., Condit, R., Dalling, J. W., Davies, S. J., Diaz, S., Engelbrecht, B. M. J., Harms, K. E., Hubbell, S. P., Marks, C. O., Ruiz-Jaen, M. C., Salvador, C. M., and Zanne, A. E.: Functional traits and the growth-mortality trade-off in tropical trees, Ecology, 91, 3664-3674, Doi 10.1890/09-2335.1, 2010.
Xu, C. G. and Gertner, G.: Understanding and comparisons of different sampling approaches for the Fourier Amplitudes Sensitivity Test (FAST), Comput Stat Data An, 55, 184-198, 10.1016/j.csda.2010.06.028, 2011a.
Xu, C. G. and Gertner, G. Z.: Reliability of global sensitivity indices, J Stat Comput Sim, 81, 1939-1969, 10.1080/00949655.2010.509317, 2011b.
Xu, C. G., McDowell, N. G., Fisher, R. A., Wei, L., Sevanto, S., Christoffersen, B. O., Weng, E. S., and Middleton, R. S.: Increasing impacts of extreme droughts on vegetation productivity under climate change, Nat Clim Change, 9, 948-+, 10.1038/s41558-019-0630-6, 2019.
Xu, X. T., Medvigy, D., Powers, J. S., Becknell, J. M., and Guan, K. Y.: Diversity in plant hydraulic traits explains seasonal and inter-annual variations of vegetation dynamics in seasonally dry tropical forests, New Phytol, 212, 80-95, 10.1111/nph.14009, 2016.
Yang, S. D. and Tyree, M. T.: Hydraulic Resistance in Acer-Saccharum Shoots and Its Influence on Leaf Water Potential and Transpiration, Tree Physiol, 12, 231-242, DOI 10.1093/treephys/12.3.231, 1993.